

# Biophysical regulation of epigenetic state and cell reprogramming

Timothy L. Downing<sup>1,2</sup>, Jennifer Soto<sup>1,2</sup>, Constant Morez<sup>2,3†</sup>, Timothee Houssin<sup>2,4†</sup>, Ashley Fritz<sup>5</sup>, Falei Yuan<sup>2,6</sup>, Julia Chu<sup>2</sup>, Shyam Patel<sup>2</sup>, David V. Schaffer<sup>1,2,5</sup> and Song Li<sup>1,2★</sup>

**Biochemical factors can help reprogram somatic cells into pluripotent stem cells, yet the role of biophysical factors during reprogramming is unknown. Here, we show that biophysical cues, in the form of parallel microgrooves on the surface of cell-adhesive substrates, can replace the effects of small-molecule epigenetic modifiers and significantly improve reprogramming efficiency. The mechanism relies on the mechanomodulation of the cells' epigenetic state. Specifically, decreased histone deacetylase activity and upregulation of the expression of WD repeat domain 5 (WDR5)—a subunit of H3 methyltransferase—by microgrooved surfaces lead to increased histone H3 acetylation and methylation. We also show that microtopography promotes a mesenchymal-to-epithelial transition in adult fibroblasts. Nanofibrous scaffolds with aligned fibre orientation produce effects similar to those produced by microgrooves, suggesting that changes in cell morphology may be responsible for modulation of the epigenetic state. These findings have important implications in cell biology and in the optimization of biomaterials for cell-engineering applications.**

Cell reprogramming represents a major advancement in cell biology and has wide applications in regenerative medicine, disease modelling and drug screening. Induced pluripotent stem cells (iPSCs) can be produced from somatic cells by the forced expression of four or fewer transcription factors (for example, Oct4 (O), Sox2 (S), Klf4 (K) and c-Myc (M), or Oct4, Sox2, Nanog and Lin28; refs 1–4). Recently, the overexpression of epithelial-cadherin (E-cad) was shown to replace the need for Oct4—the most critical factor of the OSKM cocktail—during cell reprogramming<sup>5</sup>. In addition, the elimination of E-cad in somatic cells prevents nuclear reprogramming to pluripotency all together<sup>6</sup>. These results corroborate the importance of the reported mesenchymal-to-epithelial transition (MET) that occurs during the reprogramming process<sup>7</sup>.

Since the first report on iPSC generation, researchers have employed numerous methods to improve reprogramming efficiency. Chemical compounds, in particular, have shown great promise in enhancing the efficiency of iPSC formation and/or eliminating the need for some oncogenic transcription factors such as c-Myc and Klf4 (refs 8–12). For example, valproic acid (VPA), a histone deacetylase (HDAC) inhibitor, was reported to increase the percentage of Oct4<sup>+</sup> cells generated during reprogramming<sup>11</sup>. Tranylcypromine hydrochloride (TCP), an inhibitor of lysine-specific demethylase, was also shown to significantly improve reprogramming efficiency<sup>9</sup>. Researchers have more recently demonstrated the ability of VPA to promote transcription-factor-free reprogramming through the overexpression of microRNAs (miRNAs), specifically the miR302/367 cluster, in mouse fibroblasts<sup>13</sup>. Interestingly, this miRNA-mediated reprogramming was shown to be dependent on VPA-induced degradation of HDAC2, suggesting that HDAC proteins act as inhibitors of cell reprogramming.

These studies, along with many others<sup>14–16</sup>, highlight the critical role of histone modifications and other epigenetic factors in cell reprogramming.

Although extensive studies have been performed on the roles of transcription factors, miRNAs and chemical compounds in cell reprogramming, the role of biophysical cues in this process has yet to be revealed. Biophysical factors (that is, the topographical and mechanical properties of cell-adhesive materials) have been shown to regulate a variety of cellular functions such as migration, proliferation and differentiation<sup>17–29</sup>. Importantly, these functions have closely related influences in a broad range of complex biological processes such as wound healing, tissue remodelling and tumour growth. There is also growing evidence that biophysical signals can be transmitted through the cytoskeleton, and into the nucleus and chromatin<sup>30,31</sup>.

In addition, some studies have demonstrated that substrate properties can help regulate adult stem cell self-renewal<sup>32,33</sup>, and an increasing number of laboratories have investigated the role of mechanotransduction in the maintenance of embryonic stem cells<sup>6,20,34–36</sup> (ESCs). These studies highlight the importance of biomechanics in the regulation of pluripotency. For example, an intact actin–myosin network is critical for the stable propagation of human ESCs. Non-muscle myosin IIA, specifically, was found to play a critical role in ESC maintenance because its inhibition, by short hairpin RNA (shRNA) knockdown or treatment with blebbistatin, downregulates the expression of E-cad, a transmembrane mechanosensor, leading to a deregulation of the pluripotency circuitry<sup>6,34</sup>. Still, it is not known whether or how the biophysical properties of cell-adhesive materials influence adult cell reprogramming, a reverse process of cell differentiation. In addition, whether mechanotransduction can induce critical epigenetic modifications

<sup>1</sup>UC Berkeley & UCSF Joint Graduate Program in Bioengineering, Berkeley/San Francisco, California 94720/94143, USA, <sup>2</sup>Department of Bioengineering, University of California, Berkeley, B108A Stanley Hall, Berkeley, California 94720-1762, USA, <sup>3</sup>Ecole Polytechnique, 91128 Palaiseau, France, <sup>4</sup>University Lille Nord de France, F-59000 Lille, France, <sup>5</sup>Department of Chemical and Biomolecular Engineering, University of California, Berkeley, California 94720-1762, USA, <sup>6</sup>Med-X Center, Shanghai Jiao Tong University, Shanghai 200030, China. <sup>†</sup>These authors contributed equally to this work.

\*e-mail: song\_li@berkeley.edu

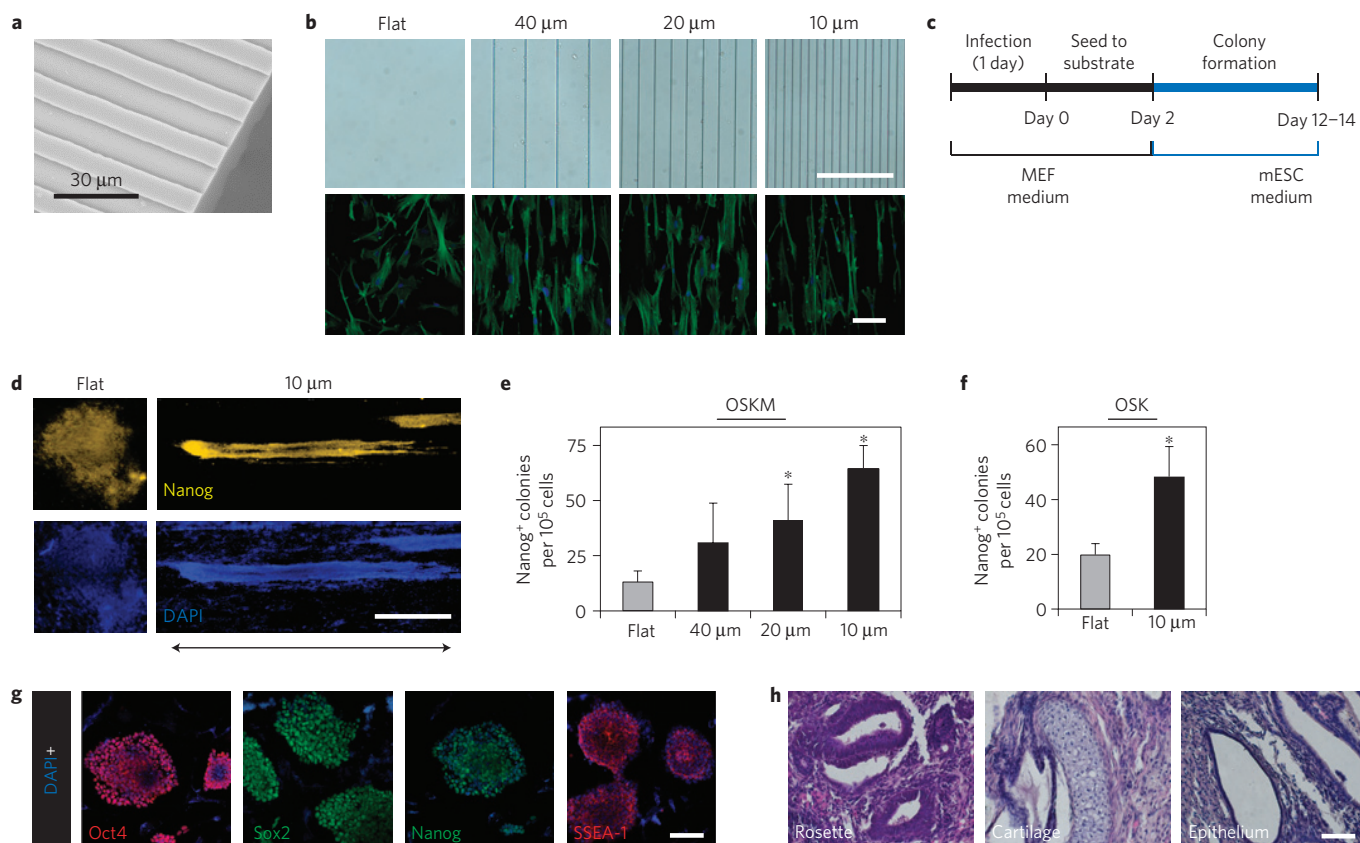


**Figure 1 | Microgroove substrates altered fibroblast morphology and improved iPSC generation.** **a**, Scanning electron micrograph of PDMS membranes with a 10 μm groove width. All grooves were fabricated with a groove height of 3 μm. **b**, The top row shows phase contrast images of flat and grooved PDMS membranes with various widths and spacings. The bottom row shows fibroblast morphology on various PDMS membranes. Images are fluorescence micrographs of the nucleus (DAPI, blue) and actin network (phalloidin, green; scale bars, 100 μm). **c**, Reprogramming protocol. Colonies were subcultured and expanded or immunostained and quantified by day 12–14. **d**, Fluorescence micrograph showing the morphology of iPSC colonies generated on flat and grooved membranes (scale bar, 1 mm). Groove dimensions were 10 μm in width and spacing, denoted as 10 μm in this and the rest of the figures. Double-headed arrow indicates microgroove orientation of alignment. **e**, Reprogramming efficiency of fibroblasts transduced with OSKM and cultured on PDMS membranes with flat or grooved microtopography. The number of biological replicates,  $n$ , used for this experiment was equal to 6. Groove width and spacing were varied between 40, 20 and 10 μm. Differences of statistical significance were determined by a one-way ANOVA, followed by Tukey's post-hoc test. \* indicates significant difference ( $p < 0.05$ ) compared with the control flat surface. **f**, Reprogramming efficiency in fibroblasts transduced with OSK ( $n = 4$ ). \* $p < 0.05$  (two-tailed, unpaired  $t$ -test) compared with the control flat surface. Error bars represent one standard deviation. **g**, Immunostaining of a stable iPSC line expanded from colonies generated on 10 μm grooves. These cells express mESC-specific markers Oct4, Sox2, Nanog and SSEA-1 (scale bar, 100 μm). **h**, The expanded iPSCs in **g** were transplanted into SCID mice to demonstrate the formation of teratomas *in vivo* (scale bar, 50 μm).

in somatic cells, which might facilitate the reprogramming process, also remains unclear.

To elucidate the role of biophysical factors in cell reprogramming, we have used reprogramming technology in conjunction with various bioengineered substrates. Our data show that the biophysical microenvironment, in the form of micro- and nano-scale topography on cell-adhesive substrates, can induce pronounced changes in histone acetylation and methylation patterns, which are dependent on cell morphological changes and actin–myosin tension. These epigenetic changes can replace the effects of potent small-molecule epigenetic modifiers and significantly improve iPSC generation efficiency. Furthermore, we identify specific mediators of this epigenetic mechanomodulation. Our findings represent a significant advancement in the understanding of mechanotransduction by revealing a new relationship between the biophysical microenvironment, epigenetic mechanomodulation and cell reprogramming.

### Microtopography enhances cell reprogramming

To assess whether topography might influence the process of cell reprogramming, primary fibroblasts, isolated from adult mouse

ears, were first transduced using polycistronic lentiviral vectors, STEMCCA–loxP or STEMCCA–loxP–RedLight<sup>37</sup>, encoding reprogramming factors OSKM or OSK, respectively. Following transduction, cells were seeded onto flat poly(dimethyl siloxane) (PDMS) membranes or those fabricated with parallel microgrooves of various width and spacing (40, 20 and 10 μm). The three-dimensional structure of PDMS membranes with a 10 μm groove width is shown in Fig. 1a. Groove heights were maintained at 3 μm for all cases. As expected, microgroove substrates had a pronounced effect on fibroblast alignment and nuclear elongation (Fig. 1b). In general, cells aligned with microgrooves, and cell spreading decreased on microgrooves. In addition, nuclear shape index decreased (more elongated) as microgroove width and spacing decreased (Supplementary Fig. 1a). Cell proliferation, as quantified by EdU (5-ethynyl-2'-deoxyuridine) incorporation, also decreased slightly (Supplementary Fig. 1b).

After seeding, transduced cells were cultured in mouse ESC (mESC) culture conditions (see Fig. 1c for the reprogramming procedure). After 12–14 days, iPSC colonies were subcultured and expanded or immunostained for Nanog protein expression

and quantified. Colony formation was observed on all PDMS membranes. Interestingly, colonies formed on microgrooves exhibited a more elongated morphology relative to those formed on flat surfaces, and favoured outgrowth along the axis of groove alignment (Fig. 1d). In addition, we observed that microgroove topography significantly enhanced cell reprogramming efficiency in mouse fibroblasts transduced with OSKM, where microgrooves of 10  $\mu\text{m}$  width (and spacing) exhibited the most pronounced effect. Here, the number of Nanog<sup>+</sup> colonies observed was more than fourfold higher than that seen on flat PDMS membranes (Fig. 1e). A similar trend was observed in mouse fibroblasts infected with only 3 factors (OSK; Fig. 1f). This enhancement of reprogramming efficiency by microgrooves was also confirmed by using mouse fibroblasts isolated from Oct4–GFP reporter mice (Supplementary Fig. 2). Given that 10  $\mu\text{m}$ -width grooves showed the greatest enhancement in cell reprogramming, we used these membranes to investigate the mechanism of action during further experimentation.

To further characterize iPSCs, colonies generated on 10  $\mu\text{m}$ -width grooved substrates were isolated and expanded for at least six passages. Colonies were then immunostained to confirm their expression of mESC-specific markers Oct4, Sox2, Nanog and SSEA-1 (Fig. 1g and Supplementary Fig. 3). Before immunostaining, we observed that iPSCs generated using STEMCCA–loxP–RedLight did not exhibit mCherry fluorescence, suggesting that transgene expression was silenced after six passages (data not shown). In addition, we confirmed that the generated iPSCs were capable of forming teratomas *in vivo* (Fig. 1h) and embryoid bodies *in vitro*, with differentiation potential for all three germ layers (Supplementary Fig. 4). Consistently, we also observed a similar trend in reprogramming efficiency of normal neonatal human dermal fibroblasts (NHDFs) cultured on flat and microgrooved surfaces (Supplementary Fig. 5).

### Biophysical regulation of histone modifications

Modulation of chromatin-modifying enzymes has a direct effect on cell reprogramming<sup>16</sup>. In addition, somatic cells must undergo pronounced changes in chromatin structure to overcome the epigenetic barriers of cell reprogramming<sup>14,15</sup>. A number of these barriers as they relate to histone modifications have been well characterized. On the basis of our previous observations in mesenchymal stem cells<sup>38</sup>, we postulated that microgroove topography might increase the presence of histone H3 acetylation (AcH3) marks in adult fibroblasts, which tend to promote cell reprogramming. For this reason, we performed a western blotting analysis to monitor global changes in AcH3 and other histone marks shown to influence cell reprogramming.

Through our analysis, we found that microgrooves markedly increased global AcH3 marks in non-transduced mouse fibroblasts (Fig. 2a) in the absence of reprogramming factors. Interestingly, we also observed an increase in methylation (both di- and tri-methylation) of histone H3 at lysine 4 (H3K4me2 and H3K4me3, respectively) on microgrooved substrates relative to flat surfaces (Fig. 2a). A similar trend in histone modifications was observed in fibroblasts infected with OSKM (Supplementary Fig. 6). Confocal microscopy confirmed that this increase was localized in the nucleus (Fig. 2b). As AcH3, H3K4me2 and H3K4me3 marks are associated with transcript activation and/or critical in the early phase of reprogramming<sup>39</sup>, we performed a chromatin immunoprecipitation (ChIP)–quantitative polymerase chain reaction (qPCR) assay at the promoter regions of Oct4, Sox2 and Nanog—the key regulators of the pluripotency network. ChIP analysis revealed significant increases in AcH3 at all three promoter regions on microgrooves relative to flat surfaces. The promoter region of Nanog showed a significant increase in H3K4me2 marks, whereas the promoter region of Sox2 showed a significant increase in H3K4me3 marks (Fig. 2c). These data suggest that microgroove

topography can induce global and local changes in histone H3 acetylation and methylation that are highly favourable in the activation of reprogramming genes.

### Replacement of chemical compounds

To further test the hypothesis that the observed increases in histone H3 acetylation and methylation on microgrooves play a role in topography-enhanced cell reprogramming, we compared the microgroove effect with that of potent small-molecule epigenetic modifiers. In particular, VPA and TCP—HDAC and histone demethylase enzyme inhibitors, respectively—have been shown to greatly improve cell reprogramming efficiency<sup>9,11</sup>. Both VPA and TCP induced global increases in AcH3, H3K4me2 and H3K4me3 in our system (Fig. 2a), suggesting that VPA and TCP had some overlapping effects on histone modifications. To determine whether microgrooves and VPA or TCP have similar effects on cell reprogramming, we reprogrammed fibroblasts cultured on flat and microgrooved membranes in the absence or presence of chemical compounds—VPA and TCP, alone or combined. From this experiment, we make several noteworthy observations. As expected, VPA and TCP alone produced a significant increase in the number of Nanog<sup>+</sup> colonies observed when the cells were reprogrammed on flat membranes (Fig. 2d). Interestingly, the number of colonies generated on flat membranes in the presence of chemical compounds increased to levels comparable with that of microgrooves in the absence of VPA and TCP, indicating that microgroove substrates had a similar effect to the chemical compounds in enhancing reprogramming efficiency. In addition, VPA and TCP showed no effect on the number of Nanog<sup>+</sup> colonies formed on microgrooves, suggesting that their mechanism of action might share a similar pathway in improving reprogramming efficiency.

As VPA was shown to be necessary for the generation of miRNA-iPSCs in mouse fibroblasts<sup>13</sup>, although complete reprogramming may not be consistently achieved<sup>40</sup>, we examined the ability of microgrooved membranes to generate colonies under the forced expression of the miRNA cluster 302/367 in the absence of VPA. Remarkably, we were able to generate colonies only on microgrooves but not on flat membranes (Supplementary Fig. 7a). We were also unable to generate any colonies with VPA alone. Although our microgrooved surfaces showed the ability to form Nanog<sup>+</sup> and GFP<sup>+</sup> clones (using fibroblasts isolated from wild-type and Oct4–GFP reporter mice, respectively) (Supplementary Fig. 7b,c), we were unable to expand these iPSC-like colonies, suggesting that microgrooved surfaces could enhance the early stage of cell reprogramming, and that additional chemical or reprogramming factors may be necessary to achieve complete reprogramming into iPSCs. These results demonstrated the ability of microgroove topography to replace or mimic the effects of chemical compounds, VPA and TCP, in cell reprogramming.

### Mediators of mechanotransduction

To elucidate the upstream mechanotransduction pathways involved in the regulation of the histone H3 modifications observed, we first monitored nuclear HDAC activity in fibroblasts cultured on microgrooved or flat membranes. Indeed, nuclear HDAC activity was significantly reduced on microgrooved substrates relative to the flat surfaces (Fig. 3a), which may account for the topography-induced AcH3. Western blotting analysis was performed to examine the expression of several HDAC proteins in mouse fibroblasts. Our results indicate that microgrooves induce pronounced decreases in the expression of HDAC2 but not HDAC1 and HDAC3 (Fig. 3b). By using confocal microscopy, we observed a presence of HDAC2 specifically within the nucleus of mouse fibroblasts, which is markedly decreased on microgrooves (Fig. 3c). As miRNA-mediated reprogramming was shown to be specifically dependent

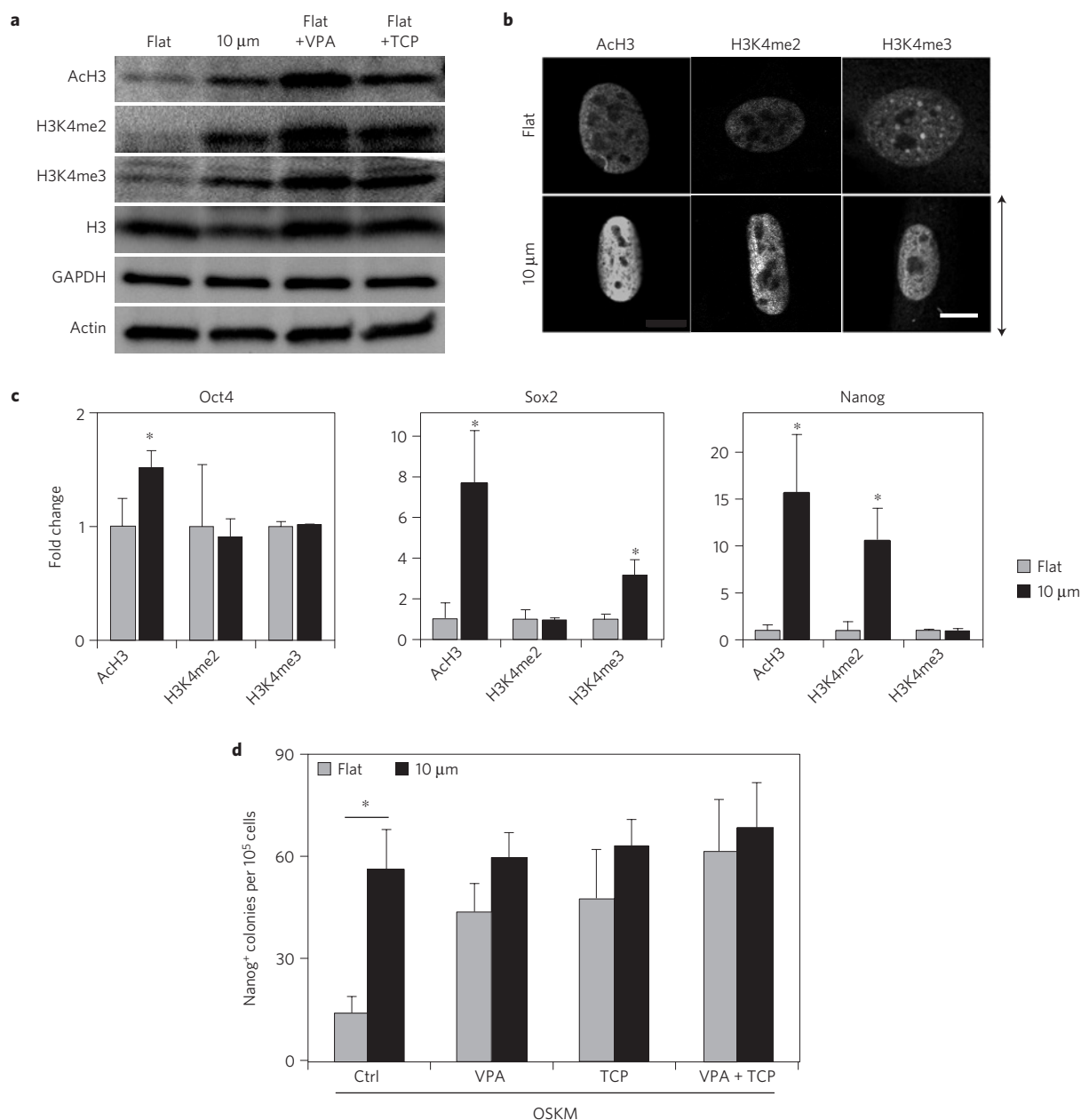


**Figure 2 | Microtopography induced histone modifications and replaced VPA and TCP in reprogramming.** **a**, Mouse fibroblasts were cultured on microgrooved or flat surfaces in the absence or presence of VPA or TCP for 3 days, followed by western blotting analysis of histone modifications AcH3, H3K4me2 and H3K4me3. Total histone H3, GAPDH and actin are shown as loading controls. **b**, Confocal microscopy shows the fluorescence intensity of histone modifications localized in the nucleus (scale bar, 10  $\mu$ m). Double-headed arrow indicates microgroove orientation of alignment. **c**, ChIP-qPCR analysis shows fold enrichment of histone modifications at the promoter regions of Oct4, Sox2 and Nanog ( $n = 3$ ). **d**, Reprogramming efficiency of fibroblasts transduced with OSKM in the presence of chemical compounds, VPA and TCP ( $n = 5$ ). \* $p < 0.05$  (two-tailed, unpaired  $t$ -test) compared with the control flat surface. Error bars represent one standard deviation.

on VPA-induced degradation of the HDAC2 protein, microgrooved topography, as with VPA, might promote the increase in global AcH3 through the downregulation of HDAC2, which may lead to the observed enhancement in cell reprogramming by OSKM and in the partial reprogramming by miRNA302/367 transduction (Fig. 1e and Supplementary Fig. 7a).

To investigate potential upstream mediators of the observed increase in H3K4 methylation on microgrooves, we screened for regulators of histone methylation. Given the recent evidence that WD repeat domain 5 (WDR5)—a subunit of H3 methyltransferase—mediates both cell reprogramming and ESC

self-renewal<sup>41</sup>, we probed for its expression through western blotting analysis and immunostaining. Interestingly, we observed that microgrooves markedly upregulated the expression of WDR5 in mouse fibroblasts (Fig. 3d,e). This result led us to perform RNA interference on WDR5 in the presence of microgrooves to determine its effects on histone modifications. Sufficient knockdown of WDR5 was confirmed at protein and gene expression levels (Fig. 3f and Supplementary Fig. 8). Surprisingly, WDR5 knockdown on grooves resulted in substantially lower levels of both H3K4me2 and H3K4me3 as well as AcH3 in mouse fibroblasts (Fig. 3f), suggesting that WDR5 plays a critical role in the modulation of both histone

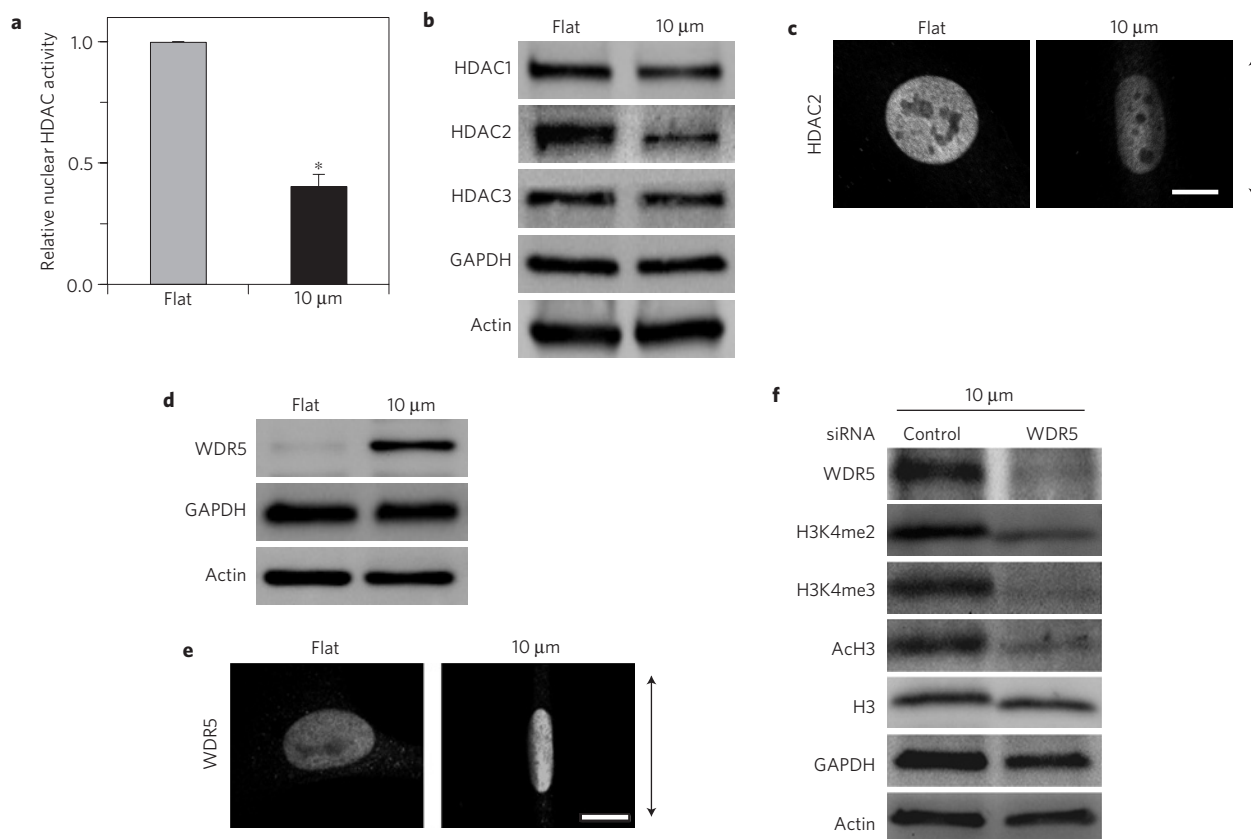


**Figure 3 | Microtopography reduced HDAC activity, downregulated HDAC2 and upregulated WDR5.** For these experiments, mouse fibroblasts were analysed after being cultured on flat or microgrooved surfaces for 3 days. **a**, Nuclear HDAC activity assay ( $n = 3$ ). \* $P < 0.05$  (two-tailed, unpaired  $t$ -test) compared with the control flat surface. Error bars represent one standard deviation. **b**, Western blotting analysis of HDACs. **c**, Confocal microscopy of HDAC2 staining. **d**, Western blotting analysis of WDR5. **e**, Confocal microscopy of WDR5. **f**, Western blotting analysis performed on fibroblasts cultured on microgrooves after siRNA knockdown of WDR5. (Scale bars in **c,e**, 10  $\mu\text{m}$ .) Double-headed arrows indicate microgroove orientation of alignment.

methylation and acetylation marks. This result also presents a new role for WDR5 as a key mediator of mechanotransduction.

### The mesenchymal-to-epithelial transition

MET is required for nuclear reprogramming in mouse fibroblasts<sup>7</sup>. In addition, a number of studies have implicated the roles of both HDAC2 and WDR5 in the expression of several epithelial and mesenchymal-associated genes<sup>42,43</sup>. For these reasons, we monitored the effect of microgroove topography on the expression of several genes associated with a MET. Real-time reverse-transcription PCR (qRT-PCR) analysis of non-transduced fibroblasts cultured on microgrooves for 3 days showed increased messenger RNA (relative to those cultured on flat membranes) for several epithelial-related genes (for example, E-cad, epithelial cell adhesion molecule (*Ep-CAM*), keratin 8 (*Krt8*), occludin (*Ocln*) and claudin 3 (*Cldn3*)) and reduced mRNA for multiple mesenchymal markers (for example, transforming growth factor  $\beta$  receptor 1 (*Tgfr1*), snail homologue 1 (*Snai1*), snail homologue 2 (*Snai2*), vimentin (*Vim*) and integrin  $\beta$  1 (*Itgb1*)). This result suggests that microgroove topography promotes the initiation of a MET in adult mouse fibroblasts (Fig. 4a). In an effort to link the histone modifications observed on microgrooved surfaces to the observed increases in epithelial-related gene expression, we performed ChIP-qPCR analysis on histone H3 modifications at the promoter of E-cad. Indeed, we observed increases in the presence of H3K4me2 at the E-cad promoter (Fig. 4b). Other marks showed no detectable change (Supplementary Fig. 9), suggesting that H3K4me2 mediates the enhanced E-cad expression and MET

transition on microgrooves. Activation of transforming growth factor- $\beta$  (TGF- $\beta$ ) pathways has been shown to block MET in cell reprogramming<sup>7</sup>. To study whether the observed MET plays a role in the topographical enhancement of cell reprogramming, we tested the effect of microgrooves on cell reprogramming in the presence of TGF- $\beta$ 1. As shown in Fig. 4c, TGF- $\beta$ 1 completely blocked the enhanced reprogramming by microgroove topography. Furthermore, inhibition of the TGF- $\beta$  pathway using *Alk5i* increased reprogramming efficiency on flat surfaces as expected, but showed no synergistic behaviour in reprogramming efficiency on microgrooves (Fig. 4d). Taken together, these results suggest that the MET induced by microgrooves plays an important role in topography-enhanced cell reprogramming.

### Actin-myosin tension and epigenetic mechanomodulation

Microgroove topography facilitates pronounced cytoskeleton reorganization in fibroblasts. Still, it is not clear how or whether these cytoskeletal changes are important in the mechanomodulation of histone modifications and their upstream regulators. For this reason, we disrupted actin-myosin contractility in fibroblasts by treatment with blebbistatin, a non-muscle myosin-II inhibitor. Remarkably, blebbistatin treatment eliminates the effect of microgrooves on the epigenetic modulation of AcH3, H3K4me2 and H3K4me3 as well as the mediators HDAC2 and WDR5 (Fig. 4e). These data strongly suggest that the cytoskeleton reorganization observed in fibroblasts on microgrooves and the actin-myosin contractility are critical in this mechanomodulation of epigenetic state and thus cell reprogramming. Figure 4f summarizes the effects

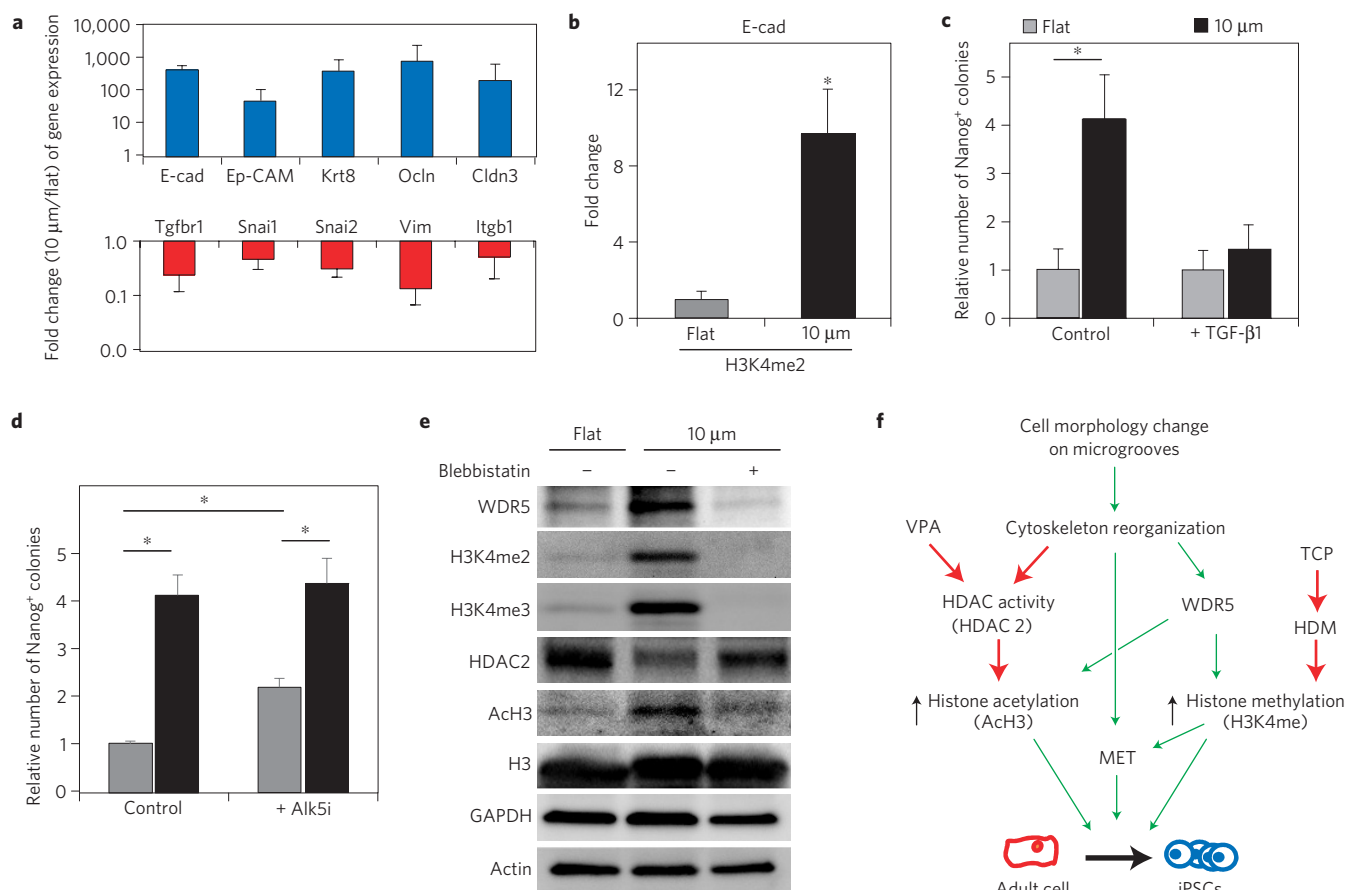


**Figure 4 | Initiation of MET and contractility-dependent histone modifications.** **a**, Mouse fibroblasts were cultured for three days on flat or microgrooved surfaces, followed by qRT-PCR analysis of epithelial-related genes and mesenchymal genes ( $n = 3$ ). **b**, ChIP-qPCR analysis for the fold enrichment of H3K4me2 modifications at the promoter region of E-cad ( $n = 3$ ).  $*p < 0.05$  (two-tailed, unpaired  $t$ -test) compared with the control flat surface. **c,d**, Mouse fibroblasts were reprogrammed with OSKM in the absence or presence of MET inhibitor, TGF- $\beta$ 1 (**c**), or TGF- $\beta$  inhibitor, A-83-01 (Alk5i) (**d**), and the number of Nanog<sup>+</sup> colonies generated was quantified ( $n = 5$  and  $n = 4$ , respectively).  $*p < 0.05$  (one-way ANOVA followed by Tukey's post-hoc test). Error bars represent one standard deviation. **e**, Western blotting analysis of mouse fibroblasts cultured on flat or microgrooved surfaces for three days in the absence or presence of blebbistatin. **f**, A summary of microtopographical regulation of histone modifications and cell reprogramming in adult mouse fibroblasts. HDM, histone demethylase.

of microgrooves on histone modifications and cell reprogramming in adult mouse fibroblasts.

### Nanoscale epigenetic regulation

Nanofibrous scaffolds can regulate cell morphology, cell organization and cell migration, as can microgrooves<sup>23,25</sup>. To generalize the role of topography in epigenetic mechanomodulation, we employed the use of nanofibrous membranes in our studies. Figure 5a shows nanofibre structure in aligned and random orientations and its effect on fibroblast morphology. As with microgrooves, aligned nanofibres encouraged fibroblast alignment and elongation over the random nanofibres. Western blotting analysis revealed that fibroblasts cultured on aligned nanofibres also exhibit global increases in AcH3, H3K4me2 and H3K4me3 marks over fibroblasts cultured on random fibres (Fig. 5b). In addition, these changes correlated well with the decrease in HDAC2 and the increase in WDR5 protein expression. Next, we seeded fibroblasts transduced with OSKM onto nanofibre surfaces to determine the effects of random and aligned fibre orientation on reprogramming efficiency. Indeed, aligned nanofibres generated significantly more Nanog<sup>+</sup> colonies than random fibres (Fig. 5c,d and Supplementary Fig. 10). These results confirm that nanofibre alignment produces an effect similar to microgrooves in epigenetic modification and cell reprogramming.

### Cell shape effect on histone modifications

A common effect of microgrooves and aligned nanofibres is cell elongation. To directly determine whether this cell-morphology change is sufficient to induce histone modifications or whether topography is required, we used micropatterning techniques to gain tight control over cell shape while culturing cells on topographically flat surfaces. Fibroblasts were cultured on micropatterned islands with well-defined cell shapes (round or elongated). Interestingly, fluorescence microscopy revealed that cells in an elongated shape (cell shape index or CSI = 0.1) exhibited significantly higher levels of nuclear AcH3, H3K4me2 and H3K4me3 as compared with cells in a circular shape (CSI = 1; Fig. 5e,f) with an equal spreading area. These data suggest that the morphological change experienced by fibroblasts, when interacting with the nano- and micro-scale features of cell-adhesive materials is sufficient to induce epigenetic modifications. Cell elongation also significantly correlated with an elongation of the cell nucleus (Supplementary Fig. 11).

Our results demonstrate, for the first time, that biophysical cues, in the form of parallel microgrooves or aligned nanofibres on the surface of cell-adhesive substrates, can significantly improve reprogramming efficiency and replace the effects of small-molecule epigenetic modifiers. The mechanism behind this biophysical enhancement of cell reprogramming relies on mechanomodulation

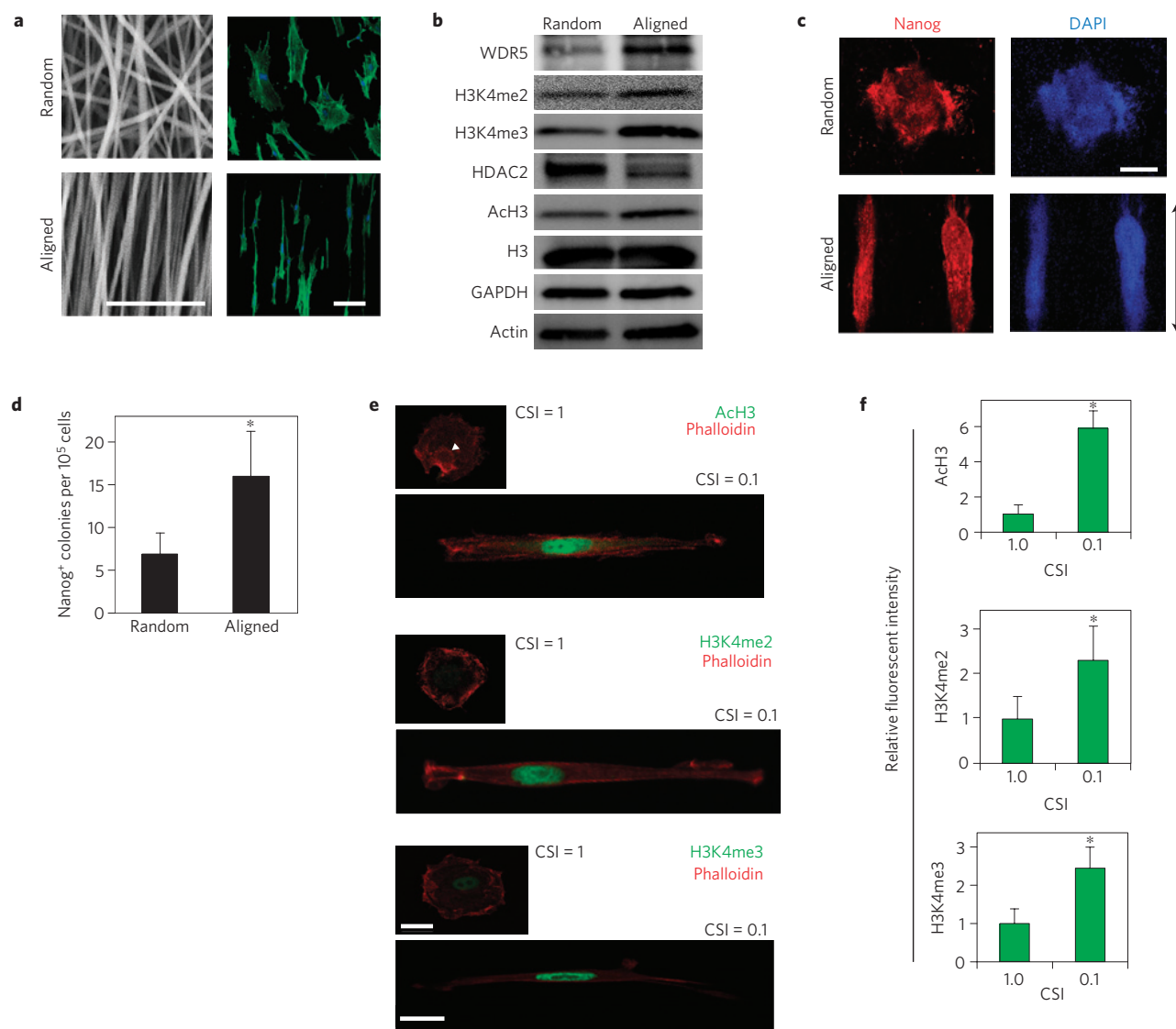


**Figure 5 | Nanoscale and morphological regulation of histone modifications and cell reprogramming.** **a**, Scanning electron micrograph of nanofibres showing fibre morphology in aligned and random orientations (scale bar, 20  $\mu\text{m}$ ). Confocal fluorescence micrograph of fibroblasts cultured on nanofibres (DAPI (blue) and phalloidin (green) staining; scale bar, 100  $\mu\text{m}$ ). **b**, Western blotting analysis for fibroblasts cultured on random and aligned nanofibres for three days. **c**, Fibroblasts were transduced with OSKM and seeded onto nanofibre surfaces, followed by immunostaining for Nanog expression (red) at day 12. Nuclei were stained with DAPI in blue; scale bar, 500  $\mu\text{m}$ . **d**, Quantification of colony numbers in **c** ( $n = 5$ ).  $*p < 0.05$  (two-tailed, unpaired  $t$ -test) compared with the control surface with random nanofibres. **e**, Fibroblasts were micropatterned into single-cell islands of 2,000  $\mu\text{m}^2$  area with a CSI value of 1 (round) or 0.1 (elongated). After 24 h, cells were immunostained for AcH3, H3K4me2 or H3K4me3 (in green). Phalloidin staining (red) identifies the cell cytoskeleton for cell shape accuracy. The white arrowhead indicates the location of the nucleus (scale bars, 20  $\mu\text{m}$ ). **f**, Quantification of fluorescence intensity in **e** ( $n = 34, 20$  and 34 for AcH3, H3K4me2 and H3K4me3, respectively).  $*p < 0.05$  (two-tailed, unpaired  $t$ -test) compared with the circular micropatterned cells (CSI = 1). Error bars represent one standard deviation.

of H3 acetylation and methylation marks, which are regulated by HDAC2 and WDR5. These epigenetic changes may also play a role in the increased expression of epithelial-related genes on microgrooved membranes. We believe this new biophysical regulation of epigenetics has important implications in the broad scope of cell biology, and provides a rational basis for the optimization of biomaterials and the cellular microenvironment for a number of biological applications.

In any given physiological microenvironment, cells may experience a number of different biophysical inputs, which, as we show, might induce critical changes in epigenetic signature. Given the broad influence of epigenetics in cell behaviour and phenotype determination, our results have interesting implications beyond

this field. It will be useful to explore, for example, whether these microtopography-induced changes in histone marks poise adult fibroblasts into a more plastic or unstable epigenetic state, allowing them to more readily transition into other phenotypes. Such evidence could greatly advance the field of cell biology by helping understand how mechanomodulated epigenetic changes alter cell behaviour in cell–material interactions, and direct cell reprogramming into cardiomyocytes and neurons<sup>44–49</sup>, tumour growth and metastasis, and adult stem/progenitor cell differentiation. This information is critical to the medical field as it presents new ways to maximize the potential of stem cell technologies, mitigate pathophysiological response in injured and diseased states, and greatly improve the design of next-generation biomaterials.

## Methods

**Fibroblast isolation, culture and reprogramming.** Ear tissues from adult C57BL/6 mice were minced and then partially digested in a solution of 3 mg ml<sup>-1</sup> collagenase type IV (Invitrogen) and 0.25% trypsin-EDTA (GIBCO) for 30 min under constant agitation at 37 °C. Partially digested tissues were plated and fibroblasts were allowed to migrate out (passage 0). Isolated fibroblasts were expanded in MEF medium (DMEM (Hyclone) +10%FBS (Hyclone) and 1% penicillin/streptomycin (GIBCO)) and used exclusively at passage 2 for all experiments. Fibroblasts from Oct4-GFP reporter mice (008214; The Jackson Laboratory) were also isolated as described above. NHDFs were purchased from Lonza (CC-2509) and expanded in FGM-2 BulletKit (CC-3132) for 1–2 passages. After transduction, mouse fibroblasts were seeded onto PDMS membranes with flat and microgroove topographies or nanofibres of aligned and random orientation. After seeding, transduced fibroblasts were maintained in MEF medium for 48 h. For the next 10–12 days, cells were fed with mouse mESC medium (DMEM +15% mouse ESC maintenance FBS (STEMCELL Technologies), 100 units ml<sup>-1</sup> ESGRO mouse leukaemia inhibitory factor (mLIF; Millipore), 0.1 mM  $\beta$ -mercaptoethanol (Sigma) and 1  $\times$  MEM non-essential amino acid (GIBCO)). Reprogrammed NHDFs were cultured in mTeSR 1 complete medium from STEMCELL Technologies. Human iPSCs were reprogrammed for 1 month after the infection with OSKM before colonies were expanded and/or analysed. Culture medium was replenished every 1–2 days during reprogramming. VPA (0.5 mM; Sigma) and TCP (5  $\mu$ M; Sigma) were used for biochemical modulation of epigenetics. Cells were exposed to TGF- $\beta$ 1 (2 ng ml<sup>-1</sup>) for 5 days for activation of the TGF- $\beta$  pathway. A-83-01 (0.5  $\mu$ M; Millipore) was used for all 14 days during the reprogramming. Blebbistatin (10  $\mu$ M; or dimethylsulphoxide) was administered for 3 days.

**Lentiviral production and cell transduction.** Lentiviral vectors were used to transduce mouse fibroblasts for ectopic expression of three (OSK) or four (OSKM) of the key reprogramming genes or miRNAs (miR302/367 cluster). STEMCCA-loxP and STEMCCA-loxP-RedLight plasmids were a generous gift from G. Mostoslavsky at Boston University. Lentivirus was produced using common, well-established calcium phosphate transfection methods. Viral particles were collected and concentrated using Lenti-X Concentrator (Clontech) according to the manufacturer's protocol. Stable virus was aliquoted and stored at -80 °C. For viral transduction, fibroblasts were seeded and allowed to attach overnight. Cells were then incubated with virus for 24 h. After incubation, transduced cells were reseeded onto either PDMS or nanofibre surfaces.

**ChIP-qPCR and qRT-PCR.** ChIP-qPCR was performed by using a high-throughput ChIP kit (EZ-Magna ChIP HT96; Millipore), according to the manufacturer's instructions. Sonicated chromatin prepared from 100,000 mouse fibroblasts was subjected to ChIP by using 3  $\mu$ g of normal rabbit IgG (CS200581; Millipore) or specific antibodies for ACh3 (06-599; Millipore), H3K4me2 (05-1338; Millipore) or H3K4me3 (07-473; Millipore). Substantial fold enrichment was observed for each experimental condition (Supplementary Fig. 12). ChIP-qPCR data were analysed by normalizing the DNA concentration to the percentage input using a relative standard curve method. Primers for ChIP-qPCR are included as (Supplementary Table 1). qRT-PCR was performed using a customized Stellaray Gene Expression System (Lonza) to probe for multiple genes at once. RNA was isolated using a NucleoSpin RNA II kit from Clontech and converted to complementary DNA using the RT<sup>2</sup> First Strand Kit (Qiagen). qRT-PCR data were analysed using the  $\Delta\Delta$ Ct method.

**RNA interference.** RNA interference was performed using control (Cat. No. 4390853) and WDR5 (Cat. No. 4390771, ID: s100547, Lot: ASO0R7L1) Silencer Select short interfering RNAs (siRNA) from Ambion. Transfections were carried out using Lipofectamine RNAiMAX Reagent (Invitrogen) according to the manufacturer's instructions.

**Western blotting analysis.** Fibroblasts were lysed and collected in a buffer containing 20 mM Tris-HCl, 150 mM NaCl, 1% Triton X-100, 0.1% SDS and 10 mM NaF along with protease inhibitors (phenylmethyl sulphonyl fluoride, Na<sub>3</sub>VO<sub>4</sub> and leupeptin). Protein lysates were centrifuged to pellet cell debris, and the supernatant was removed and quantified by DC Protein Assay (Bio-Rad). Protein samples (15 mg per well) were run using SDS-PAGE and transferred to polyvinylidene fluoride membranes. Membranes were blocked in 3% non-fat milk and incubated with primary antibodies. Primary antibodies include ACh3, H3K4me2, H3K4me3, HDAC 1, 2, 3, WDR5, H3, actin and GAPDH. Refer to Supplementary Table 2 for all antibody information. All antibodies were used at a 1:1,000 dilution and incubated overnight. Next, membranes were incubated with HRP-conjugated IgG secondary antibodies (Santa Cruz Biotechnologies) for one hour. Protein bands were visualized using Western Lightning Plus-Enhanced Chemiluminescence Substrate (Perkin Elmer Life & Analytical Sciences).

**Nuclear HDAC activity.** Nuclear HDAC activity was performed as previously described<sup>38</sup>.

## Microgroove, nanofibre and micropatterned substrate fabrication.

Bioengineered substrates were fabricated as previously described<sup>23,38,50,51</sup>. Briefly, PDMS membranes were fabricated using well-established soft lithography procedures. Poly-L-lactic acid or poly(L-lactide-co-caprolactone) nanofibres were fabricated using electrospinning technology where random fibres were ejected onto a grounded collector. Aligned fibres were produced by collector modifications or mechanical stretch. Micropatterned islands on PDMS substrates were fabricated using oxygen plasma treatment through the windows of a PDMS membrane mask that produced hydrophilic areas of different shapes and sizes. All substrates were coated with 2% gelatin for 1 h to promote cell attachment.

## Immunostaining, imaging and quantifications, teratoma formation and *in vitro* differentiation.

For immunostaining, cells were fixed with 4% paraformaldehyde, permeabilized with 0.5% Triton X-100 (Sigma) and blocked with 1% BSA (Sigma). For actin-cytoskeleton staining, samples were incubated with fluorescein-isothiocyanate-conjugated phalloidin (Invitrogen) for 2 h. Primary antibodies were incubated overnight at 4 °C, followed by 1 h incubation with Alexa 488- and/or Alexa 546-labelled secondary antibodies (Molecular Probes). Nuclei were stained with 4',6-diamino-2-phenylindole (DAPI; Invitrogen).

For counting iPSC colonies, entire wells were imaged using an ImageXpress Micro System (Molecular Devices). Colonies were determined positive for Nanog protein expression on the basis of positive (mESCs) and negative (uninfected/non-reprogrammed mouse fibroblasts) thresholds. Confocal and epifluorescence images were collected using a Zeiss LSM710 microscope and Zeiss Axio Observer.A1, respectively. DAPI images were used to determine nuclear shape index. For quantification of ACh3, H3K4me2 and H3K4me3 fluorescence intensity,  $\times 40$  epifluorescence images were used. DAPI staining was used as a mask and fluorescence intensity was averaged over the entire nucleus. All image analyses were performed using a Matlab script or ImageJ software.

Teratoma formation was performed by injecting  $1 \times 10^6$  cells into the abdominal cavity of SCID/NOD mice. After 1 month mice were euthanized, and the formed teratomas were explanted and fixed using paraffin-embedding and sectioned using a microtome. Haematoxylin and eosin staining was performed for histological analysis.

Embryoid body formation for *in vitro* differentiation was performed using the hanging-drop method. Mouse iPSCs were cultured in mESC maintenance media without LIF. Embryoid bodies were plated onto gelatin-coated surfaces and allowed to spontaneously differentiate. After 2 weeks of differentiation, samples were fixed and immunostained. Human iPSCs were overgrown in a feeder-free system using mTeSR 1 complete medium to initiate spontaneous differentiation.

**Statistical analysis.** All data are presented as mean, plus one standard deviation, where  $n \geq 3$ . Comparisons among values for groups greater than two were performed using a one-way analysis of variance (ANOVA). Differences between groups were then determined using Tukey's post-hoc test. For two-group analysis, a two-tailed, unpaired *t*-test was used. For all cases, *p*-values less than 0.05 were considered statistically significant. GraphPad Prism 6.0 software was used for all statistical evaluations.

Received 5 February 2013; accepted 11 September 2013;  
published online 20 October 2013

## References

1. Takahashi, K. & Yamanaka, S. Induction of pluripotent stem cells from mouse embryonic and adult fibroblast cultures by defined factors. *Cell* **126**, 663–676 (2006).
2. Yu, J. *et al.* Induced pluripotent stem cell lines derived from human somatic cells. *Science* **318**, 1917–1920 (2007).
3. Park, I-H. *et al.* Reprogramming of human somatic cells to pluripotency with defined factors. *Nature* **451**, 141–146 (2008).
4. Wernig, M. *et al.* *In vitro* reprogramming of fibroblasts into a pluripotent ES-cell-like state. *Nature* **448**, 318–324 (2007).
5. Redmer, T. *et al.* E-cadherin is crucial for embryonic stem cell pluripotency and can replace OCT4 during somatic cell reprogramming. *EMBO Rep.* **12**, 720–726 (2011).
6. Li, D. *et al.* Integrated biochemical and mechanical signals regulate multifaceted human embryonic stem cell functions. *J. Cell Biol.* **191**, 631–644 (2010).
7. Li, R. *et al.* A mesenchymal-to-epithelial transition initiates and is required for the nuclear reprogramming of mouse fibroblasts. *Cell Stem Cell* **7**, 51–63 (2010).
8. Feng, B., Ng, J-H., Heng, J-C. D. & Ng, H-H. Molecules that promote or enhance reprogramming of somatic cells to induced pluripotent stem cells. *Cell Stem Cell* **4**, 301–312 (2009).
9. Li, Y. *et al.* Generation of iPSCs from mouse fibroblasts with a single gene, Oct4, and small molecules. *Cell Res.* **21**, 196–204 (2011).
10. Huangfu, D. *et al.* Induction of pluripotent stem cells from primary human fibroblasts with only Oct4 and Sox2. *Nature Biotechnol.* **26**, 1269–1275 (2008).

11. Huangfu, D. *et al.* Induction of pluripotent stem cells by defined factors is greatly improved by small-molecule compounds. *Nature Biotechnol.* **26**, 795–797 (2008).
12. Zhu, S. *et al.* Reprogramming of human primary somatic cells by OCT4 and chemical compounds. *Cell Stem Cell* **7**, 651–655 (2010).
13. Anokye-Danso, F. *et al.* Highly efficient miRNA-mediated reprogramming of mouse and human somatic cells to pluripotency. *Cell Stem Cell* **8**, 376–388 (2011).
14. Pasque, V., Jullien, J., Miyamoto, K., Halley-Stott, R. P. & Gurdon, J. B. Epigenetic factors influencing resistance to nuclear reprogramming. *Trends Genet.* **27**, 516–525 (2011).
15. Plath, K. & Lowry, W. E. Progress in understanding reprogramming to the induced pluripotent state. *Nature Rev. Genet.* **12**, 253–265 (2011).
16. Onder, T. T. *et al.* Chromatin-modifying enzymes as modulators of reprogramming. *Nature* **483**, 598–602 (2012).
17. Engler, A. J., Sen, S., Sweeney, H. L. & Discher, D. E. Matrix elasticity directs stem cell lineage specification. *Cell* **126**, 677–689 (2006).
18. Paszek, M. J. *et al.* Tensional homeostasis and the malignant phenotype. *Cancer Cell* **8**, 241–254 (2005).
19. McBeath, R., Pirone, D. M., Nelson, C. M., Bhadriraju, K. & Chen, C. S. Cell shape, cytoskeletal tension, and RhoA regulate stem cell lineage commitment. *Dev. Cell* **6**, 483–495 (2004).
20. Chowdhury, F. *et al.* Material properties of the cell dictate stress-induced spreading and differentiation in embryonic stem cells. *Nature Mater.* **9**, 82–88 (2010).
21. Engler, A. J., Humbert, P. O., Wehrle-haller, B. & Weaver, V. M. Multiscale modeling of form and function. *Science* **324**, 208–212 (2009).
22. DuFort, C. C., Paszek, M. J. & Weaver, V. M. Balancing forces: Architectural control of mechanotransduction. *Nature Rev.* **12**, 308–319 (2011).
23. Patel, S. *et al.* Bioactive nanofibers: Synergistic effects of nanotopography and chemical signaling on cell guidance. *Nano Lett.* **7**, 2122–2128 (2007).
24. Thakar, R. G., Ho, F., Huang, N. F., Liepmann, D. & Li, S. Regulation of vascular smooth muscle cells by micropatterning. *Biochem. Biophys. Res. Commun.* **307**, 883–890 (2003).
25. Huang, N. F. *et al.* Myotube assembly on nanofibrous and micropatterned polymers. *Nano Lett.* **6**, 537–542 (2006).
26. Park, J. S. *et al.* The effect of matrix stiffness on the differentiation of mesenchymal stem cells in response to TGF- $\beta$ . *Biomaterials* **32**, 3921–3930 (2011).
27. Guilak, F. *et al.* Control of stem cell fate by physical interactions with the extracellular matrix. *Cell Stem Cell* **5**, 17–26 (2009).
28. Discher, D. E., Mooney, D. J. & Zandstra, P. W. Growth factors, matrices, and forces combine and control stem cells. *Science* **324**, 1673–1677 (2009).
29. Wozniak, M. A. & Chen, C. S. Mechanotransduction in development: A growing role for contractility. *Nature Rev.* **10**, 34–43 (2009).
30. Wang, N., Tytell, J. D. & Ingber, D. E. Mechanotransduction at a distance: Mechanically coupling the extracellular matrix with the nucleus. *Nature Rev.* **10**, 75–82 (2009).
31. Poh, Y.-C. *et al.* Dynamic force-induced direct dissociation of protein complexes in a nuclear body in living cells. *Nature Commun.* **3**, 866 (2012).
32. McMurray, R. J. *et al.* Nanoscale surfaces for the long-term maintenance of mesenchymal stem cell phenotype and multipotency. *Nature Mater.* **10**, 637–644 (2011).
33. Gilbert, P. M. *et al.* Substrate elasticity regulates skeletal muscle stem cell self-renewal in culture. *Science* **329**, 1078–1081 (2010).
34. Li, D. *et al.* Role of mechanical factors in fate decisions of stem cells. *Regen Med.* **6**, 229–240 (2011).
35. Chowdhury, F. *et al.* Soft substrates promote homogeneous self-renewal of embryonic stem cells via downregulating cell-matrix tractions. *PLoS ONE* **5**, e15655 (2010).
36. Ji, L., LaPointe, V. L. S., Evans, N. D. & Stevens, M. M. Changes in embryonic stem cell colony morphology and early differentiation markers driven by colloidal crystal topographical cues. *Europ. Cells Mater.* **23**, 135–146 (2012).
37. Sommer, C. A. *et al.* Excision of reprogramming transgenes improves the differentiation potential of iPS cells generated with a single excisable vector. *Stem Cells* **28**, 64–74 (2010).
38. Li, Y. *et al.* Biophysical regulation of histone acetylation in mesenchymal stem cells. *Biophys. J.* **100**, 1902–1909 (2011).
39. Buganim, Y., Faddah, D. a & Jaenisch, R. Mechanisms and models of somatic cell reprogramming. *Nature Rev. Genet.* **14**, 427–439 (2013).
40. Tavernier, G., Mlody, B., Demeester, J., Adjaye, J. & De Smedt, S. C. Current methods for inducing pluripotency in somatic cells. *Adv. Mater.* **25**, 2765–2771 (2013).
41. Ang, Y.-S. *et al.* WDR5 mediates self-renewal and reprogramming via the embryonic stem cell core transcriptional network. *Cell* **145**, 183–197 (2011).
42. Peinado, H., Ballestar, E., Esteller, M. & Cano, A. Snail mediates E-cadherin repression by the recruitment of the Sin3A/histone deacetylase 1 (HDAC1)/HDAC2 complex. *Mol. Cell. Biol.* **24**, 306–319 (2004).
43. Wu, M.-Z. *et al.* Interplay between HDAC3 and WDR5 is essential for hypoxia-induced epithelial-mesenchymal transition. *Mol. Cell* **43**, 811–822 (2011).
44. Zhou, Q., Brown, J., Kanarek, A., Rajagopal, J. & Melton, D. A. *In vivo* reprogramming of adult pancreatic exocrine cells to beta-cells. *Nature* **455**, 627–632 (2008).
45. Ieda, M. *et al.* Direct reprogramming of fibroblasts into functional cardiomyocytes by defined factors. *Cell* **142**, 375–386 (2010).
46. Pang, Z. P. *et al.* Induction of human neuronal cells by defined transcription factors. *Nature* **476**, 220–223 (2011).
47. Karow, M. *et al.* Reprogramming of pericyte-derived cells of the adult human brain into induced neuronal cells. *Cell Stem Cell* **11**, 471–476 (2012).
48. Thier, M. *et al.* Direct conversion of fibroblasts into stably expandable neural stem cells. *Cell Stem Cell* **10**, 473–479 (2012).
49. Qian, L. *et al.* *In vivo* reprogramming of murine cardiac fibroblasts into induced cardiomyocytes. *Nature* **485**, 593–598 (2012).
50. Downing, T. L. *et al.* Drug-eluting microfibrous patches for the local delivery of ropivacaine in spinal cord repair. *J. Control Release* **161**, 910–917 (2012).
51. Cheng, Q., Komvopoulos, K. & Li, S. Surface chemical patterning for long-term single-cell culture. *J. Biomed. Mater. Res. A* **96**, 507–512 (2011).

## Acknowledgements

This work is supported in part by grants from the California Institute of Regenerative Medicine (RB3-05232) and the National Institute of Health (EB012240; to S.L.), fellowships from the Ford Foundation and Siebel Scholars Foundation (to T.L.D.), a fellowship from the National Science Foundation GRFP (to J.S.), and the Fulbright-France Commission (to T.H.). The authors would like to thank M. West at the CIRM/QB3 Shared Stem Cell Facility of UC Berkeley, I. Conboy, D. Wang, C. Elabd, T. Yamaguchi, C. W. Huang, I. Grubisic, W. C. Huang, E. Su, A. Chang and J. Zhang for their assistance and fruitful discussions. The pLOVE 302/367 plasmid was provided by the laboratory of R. Belloch.

## Author contributions

S.L., T.L.D., J.S., C.M., T.H. and D.V.S. designed the experiments. T.L.D., J.S., C.M., T.H., F.Y., J.C., A.F. and S.P. carried out experiments and analysed the data. S.L., T.L.D. and J.S. wrote the manuscript.

## Additional information

Supplementary information is available in the [online version of the paper](#). Reprints and permissions information is available online at [www.nature.com/reprints](http://www.nature.com/reprints). Correspondence and requests for materials should be addressed to S.L.

## Competing financial interests

The authors declare no competing financial interests.